The Potential Application of $B_{24}N_{24}$ Cage in Li-, Na-, K-, and Mg-Ion Batteries: A DFT Investigation

[1]Shuailing Ma, [1]Junkai Wang* and [2]Zhenxia Huang

[1]*School of Materials Science and Engineering, Henan Polytechnic University, Jiaozuo, Henan Province 454003, China.*

[2]*College of Chemistry and Chemical Engineering, Henan Polytechnic University, Jiaozuo, Henan Province 454003, China.*

jkwang@hpu.edu.cn*

Summary: The potential applications of the $B_{24}N_{24}$ cage in Li-, Na-, K-, and Mg-ion batteries (LIBs, SIBs, PIBs, and MgIBs) were explored using density functional theory. Three potential adsorption sites of M/M^{q+} (M=Li, Na, K, and Mg) on the $B_{24}N_{24}$ cage were identified: above the tetragonal, hexagonal, and octagonal rings. In the case of the octagonal ring, the storage capacity of MgIBs was found to be 536 mAhg^{-1}, surpassing that of LIBs, SIBs, and PIBs with a value of 268 mAgh^{-1}. Furthermore, the sequence of cell voltages (V_{cell}) generated by the $B_{24}N_{24}$ cage in ion batteries was determined as follows: MgIBs (3.46 V) > LIBs (1.33 V) > SIBs (1.11 V) > PIBs (0.18 V). In both the tetragonal and hexagonal ring cases, the V_{cell} generated by the $B_{24}N_{24}$ cage were also highest in MgIBs, at 3.12 and 3.38 V, respectively. These findings indicate that the $B_{24}N_{24}$ cage could serve as a promising electrode material for MgIBs.

Keywords: $B_{24}N_{24}$ cage; Density functional theory; Ion batteries; Cell voltage.

Introduction

Environmental degradation and excessive energy consumption have prompted investigations into secondary batteries [1-4]. Since the discovery of lithium-ion batteries (LIBs), they have found broad applications in various electronic products and vehicles [5, 6]. Despite the promising performance of LIBs, concerns persist regarding their drawbacks, including low-energy storage capacity, rising costs, toxicity, and so on [5, 7-9]. Consequently, researchers have increasingly turned their attention to several new metal-ion batteries, like potassium-ion (PIBs), sodium-ion (SIBs), and magnesium-ion (MgIBs) batteries, due to their lower cost and widespread availability [10-14]. However, the selection of suitable anode materials for these ion batteries remains a challenge.

Typically, graphite is employed as lithium-ion battery (LIB) anodes material due to its safety and low cost, but it leads to a low lithium capacity (~370 mAgh^{-1}) 15. Additionally, other materials have been explored for application as anode electrodes in ion batteries. For example, graphene and transition metal oxides have been suggested as possible anodes for LIBs [16-18]. Moreover, in 2018, Sun and colleagues

19 studied phosphorene as a potential electrode material for MgIBs and obtained an average V_{cell} of 0.83 V. Xiao *et al*. 1 proposed graphene-like single-layer BSi as a potential anode material for both LIBs and MgIBs due to its excellent conductivity and other remarkable qualities.

Recently, it has been discovered that BN nanostructures possess outstanding qualities such as a broad band gap, a small dielectric constant, resistance to oxidation, and high temperature stability [20-23]. They have been successfully utilized in various applications including LIBs 24. Among BN nanomaterials, the $B_{24}N_{24}$ cage stands out as one of the most stable BN clusters, exhibiting excellent properties akin to those of bulk BN materials [25, 26]. In 2003, the $B_{24}N_{24}$ cage was synthesized by Oku *et al* 27, who described it as composed of hexagonal, tetragonal, and octagonal rings adhering to the isolated tetragonal rule. The properties and applications of the $B_{24}N_{24}$ cage as sensors, catalysts, and hydrogen storage materials have been extensively investigated [28-31]. For instance, Al-doped $B_{24}N_{24}$ cage has been reported to function as a potential sensor for lomustine drug detection 32. Moreover, Ganguly suggested that

---

synthesized $B_{24}N_{24}$ cage, with a hydrogen-gas storage capacity of 5.13 wt%, could serve as a promising hydrogen storage material 33.

However, there has been limited research on the utilization of $B_{24}N_{24}$ cage in ion batteries as an anode material. This paper, through DFT computations, pioneers in investigating the potential applications of $B_{24}N_{24}$ cage as an anode material for LIBs, SIBs, PIBs, and MgIBs, focusing on parameters including adsorption energy, theoretical capacity, electrical conductivity, V_{cell}, and more. This study has the potential to broaden the scope of applications for $B_{24}N_{24}$ cage.

Computational Methods

All calculations were conducted using the DMol³ module of the Materials Studio molecular software package [34-36]. The generalized gradient approximation (GGA) with the PBE exchange function was adopted to account for electron-electron interactions 37. To consider the influence of van der Waals forces, the DFT-D correction method was incorporated into the calculations 38. The binary polarization function (DNP) and semi-empirical pseudopotentials (DSPPs) with relativistic correction were utilized for the basis set and kernel electronic method. Convergence criteria of 1×10^{-5} Ha for energy change, 5×10^{-4} nm for maximum displacement, and 0.02 Ha·nm⁻¹ for maximum interaction force were applied.

To calculate the adsorption energy (E_{ad}) for the interaction of M/M^{q+} (M=Li, Na, K, Mg; and q=2 for Mg; q=1 for Li, Na, K) with the $B_{24}N_{24}$ cage, the following equation was utilized:

$$E_{ad} = E_{M/M^{q+}@B_{24}N_{24}} - E_{B_{24}N_{24}} - E_{M/M^{q+}} \qquad (1)$$

where $E_{B_{24}N_{24}}$ represents the energy of $B_{24}N_{24}$ cage.

$E_{M/M^{q+}}$ denotes the energy of a single M atom or M cation. $E_{M/M^{q+}@B_{24}N_{24}}$ represents the energy of a $B_{24}N_{24}$ cage that has an attached M atom or M cation.

The HOMO-LUMO energy gap (E_g) was defined as:

$$E_g = E_{LUMO} - E_{HOMO} \qquad (2)$$

In which E_{LUMO} and E_{HOMO} represent the energies of the LUMO and HOMO levels. And the change of E_g was calculated through the following formula:

$$\Delta E_g = \left[(E_{g2} - E_{g1}) / E_{g1} \right] \times 100 \qquad (3)$$

In which E_{g2} and E_{g1} are the corresponding complicated and pure values, respectively. This value reveals the electronic sensitivity of M/M^{q+} adsorption on $B_{24}N_{24}$ cage.

Results and Discussion

Structural optimization

The optimized structure of the $B_{24}N_{24}$ cage and its DOS plot are shown in Fig. 1, consistent with the empirically observed symmetry and geometry 27. Oku *et al*. found that the $B_{24}N_{24}$ cage comprises six octagons, twelve tetragons, and eight hexagons with O symmetry 27. And there are three distinct kinds of B-N bonds in $B_{24}N_{24}$ cage that are linked by rings of four and six members ([4-6]), four and eight members ([4-8]), and, six and eight members ([6-8]). The lengths of these bonds are about 1.50, 1.47, and 1.43 Å, respectively. In addition, three different types of NBN or BNB angles correlating to octagon, tetragon, and hexagon may be recognized. The angles in B-N-B and N-B-N are 130.19° and 136.04° for octagon, 81.91° and 97.25° for tetragon, and 114.81° and 123.02° for hexagon. Electronically, the calculations suggest that the E_g of $B_{24}N_{24}$ cage is around 4.73 eV, with LUMO and HOMO energies are -2.08 and -6.81eV, respectively (Table-1). Studies have shown that $B_{24}N_{24}$ cage is one of the most stable B-N materials and has structural dynamic stability [39-41].
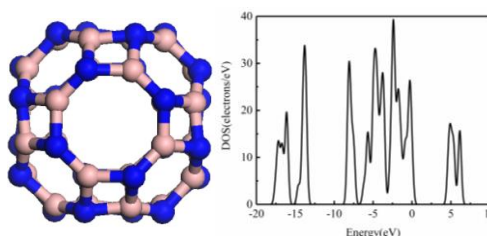

Fig. 1:   Optimized structure of $B_{24}N_{24}$ cage and its DOS.

Table-1: Adsorption energies of M/M^{q+} on the octagonal ring of B$_{24}$N$_{24}$ cage (E_{ad}), the HOMO, LUMO and energy gap (E_g) for various compounds. Energies are in eV. ΔE_g denotes the E_g change of the fullerene after atom or cation adsorption. The total energy changes (ΔE_{cell}, eV) and cell voltages (V_{cell}, V) of batteries are shown.

system	E_{ad}	E_{HOMO}	E_{LUMO}	E_g	%ΔE_g	ΔE_{cell}	V_{cell}
B$_{24}$N$_{24}$	—	-6.81	-2.08	4.73	—	—	—
B$_{24}$N$_{24}$/Li	-0.61	-6.6	-2.21	4.39	-7.19	-1.33	1.33
B$_{24}$N$_{24}$/Li$^+$	-1.93	-9.66	-5.28	4.38	-7.4		
B$_{24}$N$_{24}$/Na	-0.31	-6.62	-2.16	4.46	-5.71	-1.12	1.11
B$_{24}$N$_{24}$/Na$^+$	-1.43	-9.48	-5.06	4.42	-6.55		
B$_{24}$N$_{24}$/K	-0.78	-6.34	-1.94	4.4	-6.98	-0.18	0.18
B$_{24}$N$_{24}$/K$^+$	-0.96	-9.29	-4.85	4.44	-6.13		
B$_{24}$N$_{24}$/Mg	-0.10	-4.36	-2.08	2.28	-51.80	-6.91	3.46
B$_{24}$N$_{24}$/Mg^{2+}	-7.01	-12.52	-10.69	1.83	-61.31		

Li, Na, K, and Mg adsorption on B$_{24}$N$_{24}$ cage

Several structures of metal (M, M=Li, Na, K, Mg) atom adsorption on the B$_{24}$N$_{24}$ cage were investigated. The M atoms were positioned on the N or B atoms of the cage, on B-N bonds from distinct positions, and on various rings. After structural optimization, three possible adsorption sites were discovered, as shown in Fig. 2, which exhibited local minima on tetragonal, hexagonal, and octagonal rings.

Subsequently, the adsorption of M on the octagonal ring was explored. In this conFiguration, the adsorption energies were determined to be -0.61, -0.31, -0.78, and -0.10 eV for Li@B$_{24}$N$_{24}$, Na@B$_{24}$N$_{24}$, K@B$_{24}$N$_{24}$, and Mg@B$_{24}$N$_{24}$, respectively. The negative values of the adsorption energies (E_{ad}) imply that the complexes possess significant stability and can effectively inhibit dendrite formation on the electrode surfaces. It was also observed that the local structural changes caused by the adsorption of the B$_{24}$N$_{24}$ cage were minimal. In other words, the B$_{24}$N$_{24}$ cage can maintain its original structure following the adsorption of M atoms, which is an important characteristic for an electrode material.

Additionally, PDOS plots for M-adsorbed B$_{24}$N$_{24}$ cage were generated, as pictured in Fig. 3. These plots reveal a significant overlap between the M atom and B$_{24}$N$_{24}$ cage states around the Fermi level, indicating better stability and stronger atom adsorption on the octagonal ring of the B$_{24}$N$_{24}$ cage.

Li$^+$, Na$^+$, K$^+$, and Mg^{2+} adsorption on B$_{24}$N$_{24}$ cage

To investigate the adsorption of metal cations (M^{q+}, q=2 for Mg; q=1 for Li, Na, and K) on the B$_{24}$N$_{24}$ cage, various potential adsorption sites were examined, leading to the discovery of three local minima, similar to the adsorption of M atoms. The tetragonal, hexagonal, and octagonal rings all exhibited high structural stability

when M^{q+} were absorbed onto them. In this study, the adsorption of M^{q+} on the octagonal ring was prioritized.

The absorption of M^{q+} on the octagonal ring of the B$_{24}$N$_{24}$ cage is depicted in Fig. 2. The adsorption energies of Li$^+$, Na$^+$, and K$^+$ on the B$_{24}$N$_{24}$ cage are approximately -1.93, -1.43, and -0.96 eV, respectively (Table-1), slightly higher than those of Li, Na, and K atoms. In contrast, the E_{ad} of Mg^{2+} is significantly higher than that of Mg atoms. This suggests that due to the strong charge concentration of Mg^{2+}, there is a substantial interaction between Mg^{2+} and the B$_{24}$N$_{24}$ cage, whereas the interaction with Mg atoms is more modest. Additionally, it indicates that the structure exhibits greater stability following Mg^{2+} cation adsorption, making the development of dendrites on the electrode surface more challenging.

To evaluate how cation adsorption affects the electrical properties of the B$_{24}$N$_{24}$ cage, the results of the HOMO/LUMO energy gap (E_g) were calculated, as shown in Table-1. In these complexes, after Mg^{2+} cation adsorption, the E_g of the B$_{24}$N$_{24}$ cage is significantly reduced (by approximately 61.31%) compared to Li$^+$, Na$^+$, and K$^+$ adsorption (approximately 7.40%, 6.55%, and 6.13%, respectively). It is well-known that the conductivity of a material is mostly determined by the E_g; at a given temperature, smaller E_g values may result in higher conductance [42, 43]. Their relationship can be described by the formula:

$$\sigma = AT^{3/2} exp(-\frac{E_g}{2K_B T}) \qquad (4)$$

Where σ, A, T, and K represent the electrical conductivity, a constant, the working temperature, and the Boltzmann constant, respectively. Therefore, after the adsorption of these cations, the B$_{24}$N$_{24}$ cage undergoes a transition from being an insulator to a semiconductor, significantly increasing its conductivity. Enhanced conductivity can not only reduce the internal resistance of the battery but also minimize the generation of Joule heat during charging and discharging, thereby

significantly influencing battery performance. According to Table-1, the E_g value of the $B_{24}N_{24}$ cage decreases the most after the adsorption of Mg^{2+} cations. Hence, the $B_{24}N_{24}$ cage exhibits superior conductivity as the negative pole of MgIBs, implying its potential utility as an anode material in MgIBs.

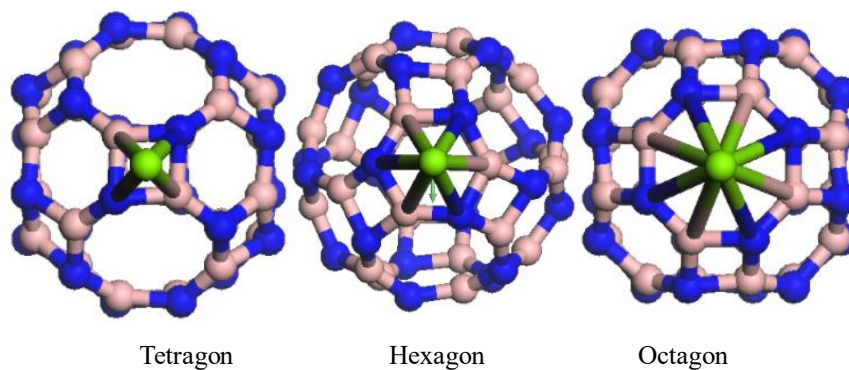Tetragon   Hexagon   Octagon

Fig. 2:   Three possible adsorption sites of M/M^{q+} on $B_{24}N_{24}$ cage.
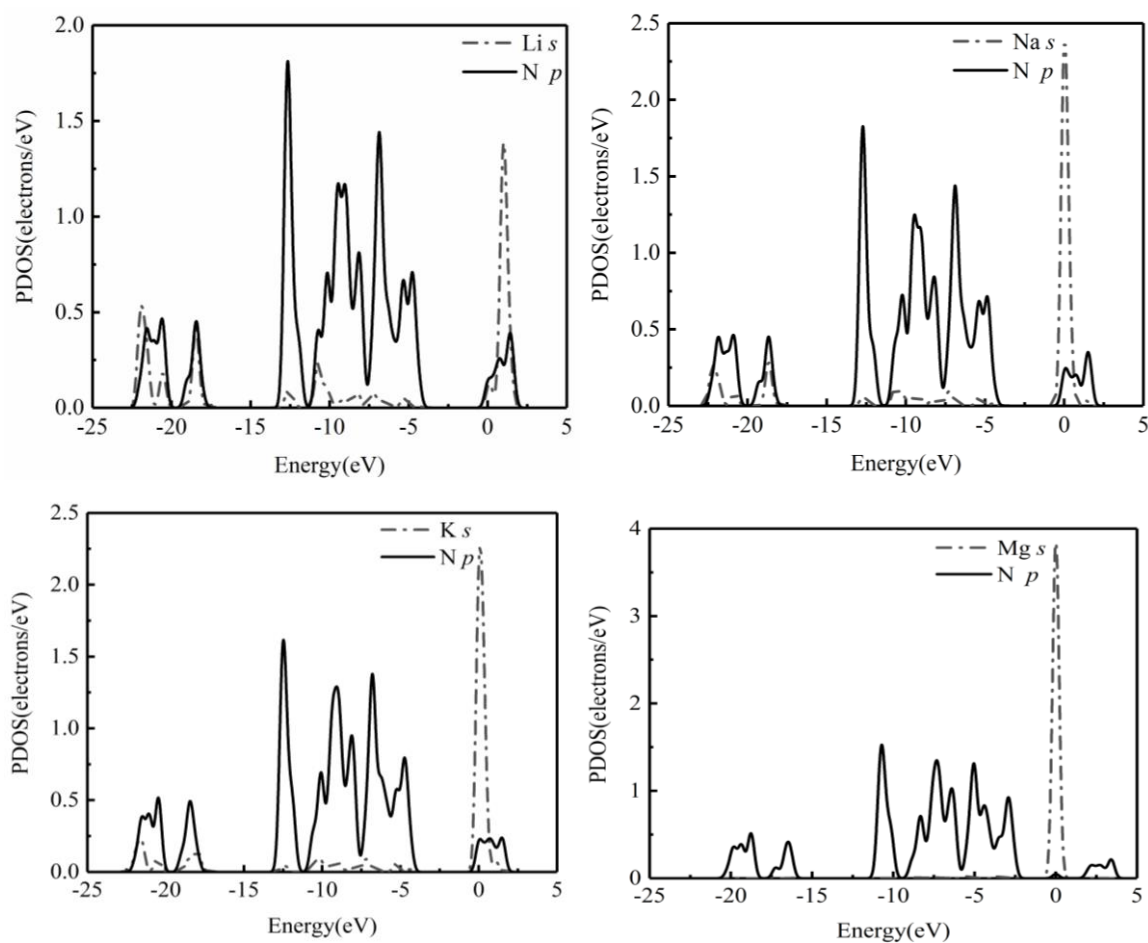

Fig. 3:   Partial density of states (PDOS) plots of $B_{24}N_{24}$ system after Li, Na, K, and Mg atom adsorption.

*Theoretical capacity of $B_{24}N_{24}$ cage*

Next, the theoretical capacity of the $B_{24}N_{24}$ cage was determined, which is a key consideration in assessing battery performance. The theoretical capacity can be determined by employing the following expression.

$$C = \frac{(n_{max} qF)}{M_{B_{24}N_{24}}} \quad (5)$$

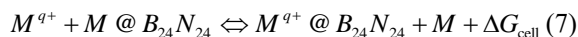Where n_{max}, q, F (Faraday constant, 26801 mAh/mol), and M_{B24N24} represent the largest number of absorbed M atoms, valence electron number, Faraday constant, and molar mass of the $B_{24}N_{24}$ cage, respectively. Based on the geometry of the $B_{24}N_{24}$ cage, it is predicted that up to six atoms can be simultaneously absorbed on the $B_{24}N_{24}$ cage. Therefore, the theoretical capacities of the $B_{24}N_{24}$ cage for Li, Na, K, and Mg are 268 and 536 mAhg^{-1} (based on $Li_6B_{24}N_{24}$, $Na_6B_{24}N_{24}$, $K_6B_{24}N_{24}$, and $Mg_6B_{24}N_{24}$), respectively. In comparison, the theoretical Mg capacity is considerably greater than that of g-C_3N_4 (319.2 mAhg^{-1}) [44] and close to that of C_2N (588.4 mAhg^{-1}) [44]. Conversely, the theoretical Li, Na, and K capacities of the $B_{24}N_{24}$ cage are lower compared to some anode materials. For instance, the theoretical Li capacity of the $B_{24}N_{24}$ cage is smaller than that of Ti_3C_2 (447.8 mAhg^{-1}) [45] and AlN (500.8 mAhg^{-1})[46]. The theoretical Na capacity of the $B_{24}N_{24}$ cage is significantly lower than that of B_2C (1596 mAhg^{-1}) [47] and graphene (1117 mAhg^{-1}) [48]. Thus, the $B_{24}N_{24}$ cage exhibits potential as an electrode material for MgIBs.

Cell voltage

Voltage is a critical parameter for assessing battery performance, as it directly impacts energy density and specific energy storage capacity. Utilizing the $B_{24}N_{24}$ cage as an anode in batteries involves defining reaction equations for both the anode and cathode:

$$M @ B_{24}N_{24} \Leftrightarrow M^{q+} @ B_{24}N_{24} + qe^{-} \, (anode) \quad M^{q+} + qe^{-} \Leftrightarrow M \, (cathode) \quad (6)$$
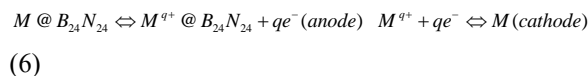
The overall reaction can be expressed as:

$$M^{q+} + M @ B_{24}N_{24} \Leftrightarrow M^{q+} @ B_{24}N_{24} + M + \Delta G_{cell} \quad (7)$$

The V_{cell} can be determined using the following equation:

$$V_{cell} = -\Delta G_{cell} / zF \quad (8)$$

$$\Delta G_{cell} = \Delta E_{cell} + P\Delta V_{cell} - T\Delta S_{cell} \quad (9)$$

Volume and entropy have minimal impact on V_{cell}, typically less than 0.01 V [49]. Therefore, excluding the terms $P\Delta V_{cell}$ $P\Delta V_{cell}$ and $T\Delta S_{cell}$ the equation simplifies to:

$$\Delta E_{cell} \square \Delta G_{cell} = E(M) + E(M^{q+} @ B_{24}N_{24}) - E(M^{q+}) - E(M @ B_{24}N_{24}) \quad (10)$$

According to this equation, ΔE_{cell} becomes more negative and larger as the interaction between M^{q+} and the $B_{24}N_{24}$ cage strengthens. A high V_{cell} may result from strong M^{q+} adsorption and weak M adsorption on the $B_{24}N_{24}$ cage. Specifically, the adsorption of Mg^{2+} on the $B_{24}N_{24}$ cage is significantly greater in Mg-ion battery compared to Mg atoms, potentially leading to a higher V_{cell}. Calculations suggest that the ΔE_{cell} and V_{cell} values are expected to be approximately -6.91 eV and 3.46 V, respectively. This V_{cell} value, while lower than $B_{24}O_{24}$ nanocage (4.45 V) [50], is higher than many of the values mentioned in recent articles in Table-2. The comparisons show the potential use of $B_{24}N_{24}$ cage as an anode material for MgIBs.

Table-2: Cell voltage (V_{cell}) values for several anode materials.

Anode materials	V_{cell} (V)	Ref
$B_{24}N_{24}$ nanocage	3.46	This work
$B_{24}O_{24}$ nanocage	4.45	50
$C_{24}N_{24}$ fullerene	2.74	53
C_{60} fullerene	3.10	13
Phosphorene	0.83	19
$B_{12}N_{12}$ nanocage	2.70	54
$B_{12}P_{12}$ nanocage	3.30	54
C_{24} nanocage	3.00	54

Table-3: Adsorption of M/M^{q+} on the tetragonal ring of $B_{24}N_{24}$ cage.

system	E_{ad}	E_{HOMO}	E_{LUMO}	E_g	%ΔE_g	ΔE_{cell}	V_{cell}
$B_{24}N_{24}$	—	-6.81	-2.08	4.73	—	—	—
$B_{24}N_{24}$/Li	-0.52	-6.5	-2.61	3.89	-17.76	-1.03	1.03
$B_{24}N_{24}$/Li$^+$	-1.56	-9.39	-5.51	3.88	-17.97		
$B_{24}N_{24}$/Na	-0.3	-6.6	-2.44	4.16	-12.05	-0.79	0.79
$B_{24}N_{24}$/Na$^+$	-1.09	-9.22	-5.63	3.59	-24.1		
$B_{24}N_{24}$/K	-0.61	-6.33	-1.98	4.35	-8.03	-0.12	0.12
$B_{24}N_{24}$/K$^+$	-0.73	-9.07	-4.90	4.17	-11.84		
$B_{24}N_{24}$/Mg	-0.11	-4.39	-2.10	2.29	-51.59	-6.32	3.12
$B_{24}N_{24}$/Mg^{2+}	-6.34	-12.36	-11.98	0.38	-91.97		

Table-4: Adsorption of M/M^{q+} on the hexagonal ring of $B_{24}N_{24}$ cage.

system	E_{ad}	E_{HOMO}	E_{LUMO}	E_g	%ΔE_g	ΔE_{cell}	V_{cell}
$B_{24}N_{24}$	—	-6.81	-2.08	4.73	—	—	—
$B_{24}N_{24}$/Li	-0.56	-6.6	-2.17	4.43	-6.34	-1.30	1.30
$B_{24}N_{24}$/Li$^+$	-1.86	-9.53	-5.25	4.28	-9.51		
$B_{24}N_{24}$/Na	-0.32	-6.62	-2.23	4.39	-7.19	-1.02	1.02
$B_{24}N_{24}$/Na$^+$	-1.33	-9.35	-5.27	4.08	-13.74		
$B_{24}N_{24}$/K	-0.69	-6.33	-1.80	4.53	-4.23	-0.20	0.20
$B_{24}N_{24}$/K$^+$	-0.89	-9.18	-4.78	4.4	-6.98		
$B_{24}N_{24}$/Mg	-0.11	-4.35	-2.10	2.25	-52.43	-6.75	3.38
$B_{24}N_{24}$/Mg^{2+}	-6.86	-12.32	-11.30	1.02	-78.44		

However, when the $B_{24}N_{24}$ cage serves as an anode material for LIBs, SIBs, and PIBs, it's worth noting that the interaction of Li$^+$, Na$^+$, and K$^+$ is less significant compared to Li, Na, and K atoms, potentially resulting in lower V_{cell} values. As expected, computed ΔE_{cell} and V_{cell} values are -1.33, -1.12, -0.18 eV and 1.33, 1.11, 0.18 V, respectively. For comparison, $B_{24}N_{24}$ cage produce lower V_{cell} values in LIBs, SIBs, and PIBs than some other anode materials. For example, in LIBs, the V_{cell} generated by the $B_{24}N_{24}$ cage is lower than that of BNG/F$^-$ (3.98 V), BNG/Cl$^-$ (1.54 V), BNG/Br$^-$ (1.62 V)51, and COF-1 covalent organic framework (6Li/Li$^+$, 3.34 V)52, while in PIBs, it is smaller than that of (5,0) AlNNT (0.90 V), AlN sheet (1.11 V)10, and N-CNC (1.24 V)5. Thus, the $B_{24}N_{24}$ cage may not be suitable as electrode material for LIBs, SIBs, and PIBs compared to MgIBs.

Furthermore, the adsorption of M/M^{q+} on $B_{24}N_{24}$ cage tetragonal and hexagonal rings was investigated. Results show that V_{cell} obtained with $B_{24}N_{24}$ cage as the electrode for MgIBs are the highest, regardless of whether M/M^{q+} is absorbed on the tetragonal or hexagonal ring, reaching 3.12 and 3.38 V, respectively. Additionally, $B_{24}N_{24}$ cage conductivity and other features in MgIBs are superior to those in other ion batteries. In conclusion, $B_{24}N_{24}$ cage emerges as a potential anode material for MgIBs.

Conclusions

The adsorption of M/M^{q+} on the $B_{24}N_{24}$ cage was explored to assess its possible application as an anode material in LIBs, SIBs, PIBs, and MgIBs. It was observed that when M/M^{q+} was absorbed on the octagonal ring, the interaction between Mg^{2+} and the $B_{24}N_{24}$ cage was much stronger compared to that with Mg atom. In contrast, the interaction between Li$^+$, Na$^+$, K$^+$ ions and the $B_{24}N_{24}$ cage was not as pronounced as that with Mg ions. This weak contact with Li$^+$, Na$^+$, and K$^+$ ions led to lower V_{cell} for LIBs (1.33 V), SIBs (1.11 V), and PIBs (0.18 V) compared to MgIBs (3.46 V). Additionally, the storage capacity of MgIBs was found to be 536 mAhg^{-1}, which is higher than that of LIBs, SIBs, and PIBs, which have a value of 268

mAgh^{-1}. Similar trends were observed when M/M^{q+} was absorbed on the tetragonal or hexagonal ring of the $B_{24}N_{24}$ cage. The $B_{24}N_{24}$ cage exhibited higher V_{cell} for MgIBs, reaching 3.12 and 3.38 V, respectively, when used as the electrode material. Furthermore, the conductivity and other relevant properties of the $B_{24}N_{24}$ cage were superior to those of other ion batteries. These findings collectively suggest that the $B_{24}N_{24}$ cage is a promising electrode material for MgIBs.

References

1. C. Xiao, X. Tang and J. Peng. Graphene-like BSi as a promising anode material for Li-and Mg-ion batteries: A first principle study. *Appl. Surf. Sci.*, **563**, 150278 (2021).

2. C. Chen, C. S. Lee and Y. Tang. Fundamental understanding and optimization strategies for dual-ion batteries: a review. *NANO-MICRO LETT*, **15**, 121 (2023).

3. L. Li, S. Jia and S. Yue. Hydrogel-stabilized zinc ion batteries: progress and outlook. *Green Chem.*, (2024).

4. X. Zhang, Y. Tang and F. Zhang. A novel aluminum–graphite dual-ion battery. *Adv. Energy Mater.*, **6**, 1502588 (2016).

5. H. M. Berenjaghi, S. Mansouri and J. Beheshtian. A DFT study on the potential application of pristine, B and N doped carbon nanocones in potassium-ion batteries. *J. Mol. Model.*, **27**, 168 (2021).

6. J. P. Rivera-Barrera, N. Muñoz-Galeano and H. O. Sarmiento-Maldonado. SoC estimation for lithium-ion batteries: Review and future challenges. *Electronics*, **6**, 102 (2017).

7. X. Wu, J. Wang and D. Fei. Lithium metal anodes for rechargeable batteries. *Energy Environ. Sci.*, **7**, 513 (2014).

8. S. Zhang, R. Shi and K. Cai. Coordination networks in accordion-like copper based metal-organic frameworks facilitate efficient catalytic strategies in high performance lithium-sulfur batteries. *J. Electroanal. Chem.*, **967**, 118468 (2024).

9. D. Ouyang, B. Liu and J. Huang. Degradation and safety performance of lithium-ion cells under high-rate charging/discharging scenarios.

PROCESS SAF ENVIRON, **185**, 76 (2024).

10. W. Pei, H. Long and X. Zhang. AlN nanotubes and nanosheets as anode material for K-ion batteries: DFT studies. *Phys. Lett. A*, **384**, 126396 (2020).

11. X. Wang, Z. Luo and J. Huang. S/N-co-doped graphite nanosheets exfoliated via three-roll milling for high-performance sodium/potassium ion batteries. *J MATER SCI TECHNOL*, **147**, 47 (2023).

12. L. Wenkai, Z. Ning and B. Zhijie. $Na_3Zr_2Si_2PO_{12}$ ceramic electrolytes for Na-ion battery: preparation using spray-drying method and its property. *J INORG MATER*, **37**, 189 (2022).

13. E. Vessally, I. Alkorta and S. Ahmadi. A DFT study on nanocones, nanotubes (4, 0), nanosheets and fullerene C_{60} as anodes in Mg-ion batteries. *RSC Adv.*, **9**, 853 (2019).

14. M. Wang, C. Jiang and S. Zhang. Reversible calcium alloying enables a practical room-temperature rechargeable calcium-ion battery with a high discharge voltage. *Nat. Chem.*, **10**, 667 (2018).

15. J. R. Dahn, T. Zheng and Y. Liu. Mechanisms for lithium insertion in carbonaceous materials. *Science*, **270**, 590 (1995).

16. J. Hassoun, F. Bonaccorso and M. Agostini. An advanced lithium-ion battery based on a graphene anode and a lithium iron phosphate cathode. *Nano Lett.*, **14**, 4901 (2014).

17. X. Yuan, X. Li. Vanadium Hexacyanoferrate Derived V-Fe-K Mixed Oxides as Anode Materials for Lithium-Ion Batteries. *ChemistrySelect*, **5**, 13748 (2020).

18. Q. Ren, Y. Zhang and C. Liu. Hollow-sphere iron oxides exhibiting enhanced cycling performance as lithium-ion battery anodes. *ChemComm*, **55**, 11638 (2019).

19. X. Han, C. Liu and J. Sun. Density functional theory calculations for evaluation of phosphorene as a potential anode material for magnesium batteries. *RSC Adv.*, **8**, 7196 (2018).

20. S. Sayhan, A. Kinal. Computational investigation and comparison of hydrogen storage properties of $B_{24}N_{24}$ and $Al_{24}N_{24}$ nanocages. *Int. J. Hydrogen Energy*, **42**, 14166 (2017).

21. L. Feng, Y. Lu and J. Kong. Theoretical studies on the structure and properties of BN clusters (BN)n and endohedral metallo-BN clusters M@(BN)n. *Comput Theor Chem*, **964**, 56 (2011).

22. N. Karachi, A. Boshra. Alkali endohedrals of $C_{24}(BN)_{12}$ heterofullerenes: A DFT aqueous phase study. *HETEROATOM CHEM*, **29**, e21435 (2018).

23. M. Ahmadi, M. Yaghobi and F.A. Larijani. Structural, magneto, electronic and optical properties of $M@B_{24}N_{24}$ cages (M= Li, Na and K). *Indian J. Phys.*, **95**, 1735 (2021).

24. N. Tyagi, N. K. Jaiswal. Enhancing the performance of BN nanosheets as promising anode material for Li-ion batteries with carbon-doping. *J MOL GRAPH MODEL*, **115**, 108213 (2022).

25. M. Mohammad Alizadeh, F. Salimi and G. Ebrahimzadeh-Rajaei. Sensing of Sarin Nerve Agent by BN Nanoclusters: DFT and TDDFT Calculation. *Braz. J. Phys.*, **52**, 1 (2022).

26. Y. Yang, N. Ostadhosseini. A theoretical investigation on the mercaptopurine drug interaction with boron nitride nanocage: Solvent and density functional effect. *Physica E Low Dimens*, **125**, 114337 (2021).

27. T. Oku, A. Nishiwaki and I. Narita. Formation and structure of $B_{24}N_{24}$ clusters. *Chem. Phys. Lett.*, **380**, 620 (2003).

28. T. Oku. Hydrogen storage in boron nitride and carbon nanomaterials. *Energies*, **8**, 319 (2014).

29. A. Maleki. Adsorption behavior of anti-cancer procarbazine on the surface of on pristine, Al-, Si-, and C-doped $B_{24}N_{24}$ fullerenes based on the density functional theory. *Struct. Chem.*, **33**, 323 (2022).

30. F. Mamusi, D. Farmanzadeh. Solvent effect on the methanol oxidation mechanism on $B_{24}N_{24}$ nano-cage surface: A DFT-D study. *J. Mol. Liq.*, **332**, 115841 (2021).

31. R. Gholami, M. Solimannejad. Potential of $B_{24}N_{24}$ nanocluster for sensing and delivering aloe-emodin anticancer drug: A DFT study. *J. Mol. Struct.*, **1270**, 133968 (2022).

32. E. Golipour-Chobar, F. Salimi and G. Ebrahimzadeh Rajaei. Boron nitride nanocluster as a carrier for lomustine anticancer drug delivery: DFT and thermodynamics studies. *Monatsh. Chem.*, **151**, 309 (2020).

33. G. Ganguly, T. Malakar and A. Paul. In Pursuit of Sustainable Hydrogen Storage with Boron-Nitride Fullerene as the Storage Medium. *ChemSusChem*, **9**, 1386 (2016).

34. B. Delley. An all-electron numerical method for solving the local density functional for polyatomic molecules. *J. Chem. Phys.*, **92**, 508 (1990).

35. B. Delley. Fast calculation of electrostatics in crystals and large molecules. *J. Phys. Chem.*, **100**, 6107 (1996).

36. B. Delley. From molecules to solids with the DMol^3 approach. *J. Chem. Phys.*, **113**, 7756

(2000).

37. J. P. Perdew, K. Burke and M. Ernzerhof. Generalized gradient approximation made simple. *Phys. Rev. Lett.*, **77**, 3865 (1996).

38. S. Grimme. Accurate description of van der Waals complexes by density functional theory including empirical corrections. *J Comput Chem*, **25**, 1463 (2004).

39. R. R. Zope, T. Baruah and M. R. Pederson. Electronic structure, vibrational stability, infrared, and Raman spectra of $B_{24}N_{24}$ cages. *Chem. Phys. Lett.*, **393**, 300 (2004).

40. H. S. Wu, H. Jiao. What is the most stable $B_{24}N_{24}$ fullerene?. *Chem. Phys. Lett.*, **386**, 369 (2004).

41. A. R. Adabinezhad, M. Yaghobi and M. A. Ramzanpour. Optical and magneto-optical properties of the SC, FCC and BCC phases of the $B_{24}N_{24}$ crystal. *J. Mod. Opt.*, **67**, 1436 (2020).

42. S. S. Li. Scattering mechanisms and carrier mobilities in semiconductors//Semiconductor Physical Electronics. *Springer*, New York, NY, 211 (2006).

43. A. A. Peyghan, M. Noei. A theoretical study of lithium-intercalated pristine and doped carbon nanocones. *J. Am. Chem. Soc.*, **58**, 46 (2014).

44. J. Zhang, G. Liu and H. Hu. Graphene-like carbon-nitrogen materials as anode materials for Li-ion and mg-ion batteries. *Appl. Surf. Sci.*, **487**, 1026 (2019).

45. D. Er, J. Li and M. Naguib. Ti_3C_2 MXene as a high capacity electrode material for metal (Li, Na, K, Ca) ion batteries. *ACS Appl. Mater. Interfaces*, **6**, 11173 (2014).

46. A. Sengupta. Lithium and sodium adsorption properties of two-dimensional aluminum nitride. *Appl. Surf. Sci.*, **451**, 141 (2018).

47. X. Yu, X. Chen and X. Wang. Metallic B_2C monolayer as a promising anode material for

Li/Na ion storage. *Chem. Eng. J.*, **406**, 126812 (2021).

48. Z. Liang, X. Fan and W. Zheng. Adsorption and formation of small Na clusters on pristine and double-vacancy graphene for anodes of Na-ion batteries. *ACS Appl. Mater. Interfaces*, **9**, 17076 (2017).

49. Y. S. Meng, M. E. Arroyo-de Dompablo. First principles computational materials design for energy storage materials in lithium ion batteries. *Energy Environ. Sci.*, **2**, 589 (2009).

50. R. Rahimi, M. Solimannejad and M. Soleimannejad. Increasing the cell voltage of a magnesium ion battery with $B_{24}O_{24}$ anode through encapsulating halides: a DFT study. *Mol Phys*, **122**, e2252107 (2024).

51. R. Rahimi, M. Solimannejad. The potential application of borazine (B_3N_3)-doped nanographene decorated with halides as anode materials for Li-ion batteries: a first-principles study. *J. Mol. Model.*, **26**, 1 (2020).

52. M. Heidari, M. Solimannejad. A DFT study of COF-1 covalent organic framework as a disposable platform for rechargeable lithium-ion battery anodes. *Phys. Rev. B Condens*, **664**, 415027 (2023).

53. S. Ma, J. Wang and Z. Huang. A DFT study of $C_{24}N_{24}$ Fullerene as Anode Material in Li-, Na-, K-, and Mg-Ion Batteries. *J CHEM SOC PAKISTAN*, **46**, (2024).

54. E. Shakerzadeh, H. Mirzavand and Z. Mahdavifar. A comparative DFT study on prospective application of C_{24}, $Si_{12}C_{12}$, $B_{12}N_{12}$, $B_{12}P_{12}$, $Al_{12}N_{12}$, and $Al_{12}P_{12}$ nanoclusters as suitable anode materials for magnesium-ion batteries (MIBs). *PHYSICA E*, **140**, 115161 (2022).